PCCP

PAPER

View Article Online
View Journal | View Issue

Open Access Article. Published on 06 January 2015. Downloaded on 5/6/2026 12:57:53 PM.
This article is licensed under a Creative Commons Attribution 3.0 Unported Licence.

Cite this: *Phys. Chem. Chem. Phys.*, 2015, **17**, 4076

Kinetics of stabilised Criegee intermediates derived from alkene ozonolysis: reactions with SO_2, H_2O and decomposition under boundary layer conditions

Mike J. Newland,[a] Andrew R. Rickard,[b] Mohammed S. Alam,[a] Luc Vereecken,[c] Amalia Muñoz,[d] Milagros Ródenas[d] and William J. Bloss*[a]

Received 17th September 2014,
Accepted 23rd December 2014

DOI: 10.1039/c4cp04186k

www.rsc.org/pccp

The removal of SO_2 in the presence of alkene–ozone systems has been studied for ethene, *cis*-but-2-ene, *trans*-but-2-ene and 2,3-dimethyl-but-2-ene, as a function of humidity, under atmospheric boundary layer conditions. The SO_2 removal displays a clear dependence on relative humidity for all four alkene–ozone systems confirming a significant reaction for stabilised Criegee intermediates (SCI) with H_2O. The observed SO_2 removal kinetics are consistent with relative rate constants, $k(\mathrm{SCI} + H_2O)/k(\mathrm{SCI} + SO_2)$, of 3.3 (±1.1) × 10^{-5} for CH_2OO, 26 (±10) × 10^{-5} for CH_3CHOO derived from *cis*-but-2-ene, 33 (±10) × 10^{-5} for CH_3CHOO derived from *trans*-but-2-ene, and 8.7 (±2.5) × 10^{-5} for $(CH_3)_2COO$ derived from 2,3-dimethyl-but-2-ene. The relative rate constants for $k(\mathrm{SCI\ decomposition})/k(\mathrm{SCI} + SO_2)$ are −2.3 (±3.5) × 10^{11} cm^{-3} for CH_2OO, 13 (±43) × 10^{11} cm^{-3} for CH_3CHOO derived from *cis*-but-2-ene, −14 (±31) × 10^{11} cm^{-3} for CH_3CHOO derived from *trans*-but-2-ene and 63 (±14) × 10^{11} cm^{-3} for $(CH_3)_2COO$. Uncertainties are ±2σ and represent combined systematic and precision components. These values are derived following the approximation that a single SCI is present for each system; a more comprehensive interpretation, explicitly considering the differing reactivity for *syn*- and *anti*-SCI conformers, is also presented. This yields values of 3.5 (±3.1) × 10^{-4} for $k(\mathrm{SCI} + H_2O)/k(\mathrm{SCI} + SO_2)$ of *anti*-CH_3CHOO and 1.2 (±1.1) × 10^{13} for $k(\mathrm{SCI\ decomposition})/k(\mathrm{SCI} + SO_2)$ of *syn*-CH_3CHOO. The reaction of the water dimer with CH_2OO is also considered, with a derived value for $k(CH_2OO + (H_2O)_2)/k(CH_2OO + SO_2)$ of 1.4 (±1.8) × 10^{-2}. The observed SO_2 removal rate constants, which technically represent upper limits, are consistent with decomposition being a significant, structure dependent, sink in the atmosphere for *syn*-SCI.

1. Introduction

Atmospheric oxidation processes are central to understanding trace gas atmospheric composition, the abundance of air pollutants harmful to human health, crops and ecosystems, and the removal of reactive greenhouse gases such as methane. The principal atmospheric oxidants responsible for initiating the gas-phase degradation of volatile organic compounds (VOCs), NO_x and SO_2 are OH, NO_3 and O_3, with additional contributions from other species such as halogen atoms. Recent field measurements[1] in a boreal forest have identified the presence of an additional oxidant species, removing SO_2 and producing H_2SO_4. The additional SO_2 oxidation observed was substantial (comparable to that due to OH radicals alone), and attributed to a product of alkene ozonolysis – the boreal forest environment being one in which substantial biogenic alkene emissions occur – suggested to be the stabilised Criegee intermediate (SCI). The gas-phase oxidation of SO_2 in the atmosphere is of interest to climate research as it leads to formation of H_2SO_4, contributing to new particle formation and sulphate aerosol loading, in competition with condensed phase oxidation.[2] A missing mechanism for the conversion of SO_2 to H_2SO_4 could lead to model underestimation of the sulphate aerosol burden and affect radiative forcing calculations,[3] with corresponding implications for climate predictions. Enhanced SO_2 oxidation in alkene–ozone systems was first reported by Cox & Penkett[4] over forty years ago, however the precise reaction mechanism giving rise to this effect remains elusive. The ''Criegee'' ozonolysis reaction mechanism was first postulated in the 1940s.[5] It is now accepted that the ozone

[a] *University of Birmingham, School of Geography, Earth and Environmental Sciences, Birmingham, UK. E-mail: W.J.Bloss@bham.ac.uk*
[b] *Wolfson Atmospheric Chemistry Laboratories, Department of Chemistry, University of York, York, UK and National Centre for Atmospheric Science, University of York, York, UK*
[c] *Max Planck Institute for Chemistry, Atmospheric Sciences, J.-J.-Becher-Weg 27, Mainz, Belgium*
[d] *Instituto Universitario CEAM-UMH, EUPHORE Laboratories, Avda/Charles R. Darwin. Parque Tecnologico, Valencia, Spain*

 This journal is © the Owner Societies 2015

Open Access Article. Published on 06 January 2015. Downloaded on 5/6/2026 12:57:53 PM.
This article is licensed under a Creative Commons Attribution 3.0 Unported Licence.

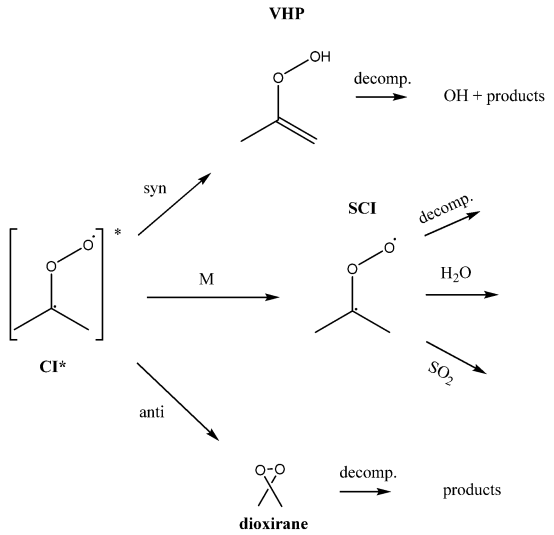

Scheme 1 Simplified mechanism for the reaction of Criegee Intermediates (SCIs) formed from alkene ozonolysis.

molecule adds to the C=C double bond *via* a concerted cycloaddition to form a primary ozonide, followed by cleavage of the C–C bond and one of the O–O bonds forming a carbonyl molecule and a carbonyl oxide, or 'Criegee intermediate' (CI).[6] Ozonolysis derived SCIs are formed with a broad internal energy distribution, to yield chemically activated and stabilised SCIs. SCIs can have sufficiently long lifetimes to undergo bimolecular reactions with H_2O and SO_2 amongst other species. Chemically activated SCIs may also undergo collisional stabilisation, unimolecular decomposition or isomerisation (Scheme 1). For substituted alkenes, SCIs can undergo a 1,4-H-shift rearrangement through a vinyl-hydroperoxide (VHP) *via* the so-called "hydroperoxide channel" and decompose to yield OH and a vinoxy radical – a substantial non-photolytic source of atmospheric oxidants.[7,8] This is the favoured channel for SCIs formed in the *syn*-configuration. Time resolved studies[9] show that the VHP may persist for appreciable timescales under boundary layer conditions, giving rise to the observed pressure dependence of OH radical yields,[10] and opening the possibility for bimolecular reactions of this species to occur. SCIs formed in the *anti*-configuration are thought to primarily undergo rearrangement and decomposition *via* a dioxirane intermediate ("the acid/ester channel"), producing a range of daughter products and contributing to the observed overall HO_x radical yield.[6,11]

$$\text{Alkene} + O_3 \xrightarrow{k_1} \phi\text{SCI} + (1-\phi)\text{CI} + \text{RCHO} \quad \text{(R1)}$$

$$\text{SCI} + SO_2 \xrightarrow{k_2} SO_3 + \text{RCHO} \quad \text{(R2)}$$

$$\text{SCI} + H_2O \xrightarrow{k_3} \text{products} \quad \text{(R3)}$$

$$\text{SCI} \xrightarrow{k_d} \text{products} \quad \text{(R4)}$$

Until recently, it has been thought that the predominant atmospheric fate for SCIs was reaction with water vapour[12,13] – leading to a significant source of organic acids and hydroperoxides, suggesting that bimolecular reaction with SCIs is an unimportant oxidation mechanism for trace gas species. This view was recently challenged by direct observation[14] and kinetic studies[15–17] of the CH_2OO and CH_3CHOO SCIs.

Taatjes and co-workers,[15] directly observing CI kinetics for the first time, found reactions of CH_2OO with SO_2 and NO_2 to be substantially faster than previously thought, pointing to a potentially important role for this species in atmospheric SO_2 and NO_2 oxidation; subsequent measurements have identified SO_3 (ref. 16) and NO_3 (ref. 18) as products of these reactions. The key to whether SCIs are indeed significant contributors to gas-phase atmospheric SO_2 oxidation is the ratio of the rate constants for reaction of the SCI with SO_2 (k_2), to that with H_2O (k_3) and decomposition (k_d). In laboratory studies where SCIs were produced by the 248 nm laser photolysis of alkyl iodide precursors at 4 Torr total pressure, with the SCI decay monitored by VUV photoionisation in the presence of excess co-reactants, this ratio has recently been reported to be 10^3–10^4 for the smallest two SCIs (CH_2OO[15,17] and CH_3CHOO[16]), with k_2 on the order of 10^{-11} cm^3 s^{-1} and k_3 on the order of 10^{-15} cm^3 s^{-1}. In contrast, alternative studies of SO_2 oxidation in alkene–ozone systems, performed at atmospheric pressure through detection of the H_2SO_4 product, find much smaller SCI + SO_2 rate coefficients (by *ca.* two orders of magnitude).[19] Explanations for this apparent discrepancy may include the lifetime of the secondary ozonide (SOZ) adduct formed from the SCI + SO_2 reaction, collisionally stabilised at atmospheric pressure,[20] effects of the presence of multiple SCI conformers with differing reactivity, or contributions from other oxidant species, formed within the ozonolysis system, to SO_2 reaction. Understanding the behaviour of the ozone–alkene–SO_2 system in the presence of water vapour is critical to quantifying the impact of SCI chemistry upon atmospheric SO_2 oxidation.[21]

An additional, potentially important, fate of SCI under atmospheric conditions is unimolecular decomposition (denoted k_d in (R4)). For CH_2OO, rearrangement *via* a 'hot' acid species represents the lowest accessible decomposition channel, but due to lack of alkyl substituents, the theoretically predicted 298 K rate constant is rather low, 0.3 s^{-1}.[22] Previous studies have identified the hydroperoxide rearrangement as dominant for SCIs with a *syn* configuration, determining their overall unimolecular decomposition rate.[7,8] For *syn*-CH_3CHOO recent experimental[23] work yielded a decomposition rate of 3–30 s^{-1}. Theoretical work[24] has predicted a decomposition rate coefficient of 24.2 s^{-1} for *syn*-CH_3CHOO and 67.2 s^{-1} for *anti*-CH_3CHOO (for which only the ester channel exists), owing to the potential energy release from the higher energy *anti*-conformer.[23] An upper limit to total CH_3CHOO loss (decomposition and heterogeneous wall losses combined) of <250 s^{-1} has been reported by Taatjes *et al.*[16] Earlier experimental work reported decomposition rate constants of ≤ 20 s^{-1} for CH_3CHOO derived from *cis*-but-2-ene ozonolysis,[25] and 76 s^{-1} (accurate to within a factor of three) for CH_3CHOO derived from *trans*-but-2-ene ozonolysis.[26] For $(CH_3)_2COO$ (derived from 2,3-dimethyl-but-2-ene ozonolysis) a total loss rate of 3.0 s^{-1} has recently been determined experimentally.[19] This value (which represents an upper limit for k_d)

Open Access Article. Published on 06 January 2015. Downloaded on 5/6/2026 12:57:53 PM.
This article is licensed under a Creative Commons Attribution 3.0 Unported Licence.

is somewhat smaller than but comparable in magnitude to an earlier measurement of 6.4 s^{-1} (determined at 100 Torr).[27] Theoretical estimates of $(CH_3)_2COO$ decomposition rates are higher, at up to 250 s^{-1}.[22] Photolysis loss rates have also recently been reported for CH_2OO[28] and CH_3CHOO[29] of 1 s^{-1} and 0.2 s^{-1} respectively, calculated for actinic flux values at midday, SZA = 0°.

Here, we present results of a series of experiments in which the oxidation of SO_2 during the ozonolysis of ethene, *cis*-but-2-ene, *trans*-but-2-ene and 2,3-dimethyl-but-2-ene (tetramethylethylene, TME), was investigated in the presence of varying amounts of water in the European Photochemical Reactor facility (EUPHORE), Valencia, Spain.

2. Experimental

2.1 EUPHORE

EUPHORE is a 200 m^3 simulation chamber used for studying reaction mechanisms under atmospheric boundary layer conditions. In general, experiments comprised time-resolved measurement of the removal of SO_2 in the presence of an alkene–ozone system, as a function of humidity. SO_2 and O_3 abundance were measured using conventional fluorescence and UV absorption monitors, respectively; alkene abundance was determined *via* FTIR spectroscopy. The precision of the SO_2 and O_3 monitors were 0.25 and 0.47 ppbv respectively (evaluated as 2 standard deviations of the measured value prior to SO_2 or O_3 addition). The chamber is fitted with large horizontal and vertical fans to ensure rapid mixing (three minutes). Further details of the chamber setup and instrumentation are available elsewhere.[30,31] Experiments were performed in the dark (*i.e.* with the chamber housing closed; $j(NO_2) \leq 10^{-6}$ s^{-1}), at atmospheric pressure (*ca.* 1000 mbar) and temperatures between 296 and 303 K, on timescales of *ca.* 20–30 minutes. Chamber dilution was monitored *via* the first order decay of an aliquot of SF_6, added prior to each experiment. Cyclohexane (*ca.* 75 ppmv) was added at the beginning of each experiment to act as an OH scavenger, such that SO_2 reaction with OH was calculated to be ≤1% of the total chemical SO_2 removal in all experiments.

2.2 Experimental approach

Experimental procedure, starting with the chamber filled with clean air, comprised addition of SF_6 and cyclohexane, followed by water vapour, O_3 (*ca.* 500 ppbv) and SO_2 (*ca.* 50 ppbv). A gap of five minutes was left prior to addition of the alkene, to allow complete mixing. The reaction was then initiated by addition of the alkene (*ca.* 500 ppbv for ethene, 200 ppbv for *cis*- and *trans*-but-2-ene and 400 ppbv for TME). The chamber was monitored for an hour subsequent to the addition of ethene and forty five minutes for *cis*- and *trans*-but-2-ene and TME. The rate of alkene–ozone consumption is dependent on k_1. Roughly 25% of the ethene was consumed after an hour, while for *cis*- and *trans*-but-2-ene and TME 90% of the alkene was consumed within roughly 25 minutes, 20 minutes and 6 minutes respectively. Each experiment was performed at a constant humidity, which was increased in a step-wise manner for consecutive runs to cover the range 1.5–21% RH. Measured increases in $[SO_2]$ agreed with measured volumetric addition across the SO_2 and humidity range used in the experiments.

2.3 Analysis approach

The following sections describe (i) a common analysis applied to all systems, but which features several approximations, and (ii) more detailed consideration of each chemical system in turn, to address potential contributions from the water dimer, and multiple criegee species within each system (*e.g.* contrasting reactivity of different SCI conformers).

From the chemistry presented in reactions (R1)–(R4) it is assumed that SCI will be produced in the chamber from the reaction of the alkene with ozone at a given yield, ϕ. The SCI produced can then react with SO_2, with H_2O, with other species or decompose under the experimental conditions applied. The rate at which SO_2 is lost, compared with the total production of SCI, is determined by the fraction, f, of the total SCI produced which reacts with SO_2, compared to the sum of the total loss processes of the SCI (eqn (E1)):

$$f = \frac{k_2[SO_2]}{k_2[SO_2] + k_3[H_2O] + k_d + L} \quad \text{(E1)}$$

$$\frac{dSO_2}{dO_3} = \phi \cdot f \quad \text{(E2)}$$

Here, L is the sum of any other pseudo-first order chemical loss processes for SCI in the chamber, after correction for dilution. (E2) neglects other (non-alkene) chemical sinks for O_3, such as reaction with HO_2 – also produced directly during alkene ozonolysis,[11] but indicated through model calculations to account for <2% of ozone loss under all the experimental conditions of this work. Eqn (E1) and (E2) treat the SCIs formed as a single species – this is the case for (*e.g.*) ethene and TME, but is an approximation for the 2-butenes; considered further below.

2.3.1 SCI yield calculation. Values for ϕ_{SCI} were determined for each ozonolysis reaction from experiments performed under dry conditions (RH < 1%) in the presence of excess SO_2 (*ca.* 1000 ppbv), such that SO_2 scavenges the overwhelming majority of the SCI. From eqn (E2), regressing dSO_2 against dO_3 (corrected for chamber dilution), assuming f to be unity (*i.e.* all the SCI produced reacts with SO_2) determines the value of ϕ_{min}, a lower limit to the SCI yield. Fig. 2 shows the experimental data, from which ϕ_{min} was derived, for all four alkene ozonolysis systems studied.

The lower limit criterion applies as in reality f will be less than one, at experimentally accessible SO_2 levels, as a small fraction of the SCI will still react with any H_2O present, or undergo decomposition. The actual yield, ϕ, was determined by combining the results from the high-SO_2 experiments with those from the series of experiments performed at lower SO_2, as a function of $[H_2O]$, to determine k_3/k_2 and k_d/k_2 (see Section 2.3.2), through an iterative process to determine the single unique value of ϕ_{SCI} which fits both datasets. It is important to note that the SCI yield is to an extent an operationally defined quantity – for example, OH formation from alkene ozonolysis is known to proceed over

Open Access Article. Published on 06 January 2015. Downloaded on 5/6/2026 12:57:53 PM.
This article is licensed under a Creative Commons Attribution 3.0 Unported Licence.

at least hundreds of milliseconds[9] following the alkene–ozone reaction, and so the corresponding CI population must also be evolving with time. In this work, SCI yields reflect the amount of SCI available to oxidise SO_2 on timescales of seconds to minutes.

2.3.2 k(SCI + H_2O)/k(SCI + SO_2) and k_d/k(SCI + SO_2). To determine k_3/k_2 and k_d/k_2, a series of experiments were performed for each alkene, in which the SO_2 loss was monitored as a function of [H_2O]. From eqn (E2), regression of the loss of ozone (dO_3) against the loss of SO_2 (dSO_2) (both corrected for dilution, measured through the removal SF_6, added at the start of each experiment and monitored *via* FTIR) for an experiment determines the factor $f\cdot\phi$ at a given point in time. This quantity will vary through the experiment as SO_2 is consumed, and other potential SCI co-reactants are produced, as predicted by eqn (E1). A smoothed fit was applied to the experimental data for the cumulative consumption of SO_2 and O_3, ΔSO_2 and ΔO_3, (Fig. 1) to determine dSO_2/dO_3 (and hence $f\cdot\phi$) at the start of each experiment, for use in eqn (E3). The start of the experiment (*i.e.* when [SO_2] ~ 50 ppbv) was used as this corresponds to the greatest rate of production of the SCI, and hence largest experimental signals (O_3 and SO_2 rate of change) and is the point at which the SCI + SO_2 reaction has the greatest magnitude compared with any other potential chemical loss processes for either species (see discussion below).

$$[SO_2]\left(\frac{1}{f}-1\right)=\frac{k_3}{k_2}[H_2O]+\frac{k_d+L}{k_2} \qquad (E3)$$

The value $[SO_2]((1/f)-1)$ can then be regressed against [H_2O] for each experiment to give a plot with a gradient of k_3/k_2 and an intercept of $(k_d + L)/k_2$ (eqn (E3)). Our data cannot determine absolute rate constants (*i.e.* values of k_2, k_3, k_d) in isolation, but is limited to assessing their relative values, which may be placed on an absolute basis through use of an (external) reference value.

Eqn (E1)–(E3) as presented above assume that only a single SCI species is present in each ozonolysis system. While this is the case for the ethene and TME systems, for the but-2-ene systems this is an approximation as two conformers of the CH_3CHOO SCI (*syn* and *anti*) are produced. Further analysis is performed in Section 3.3.2 in which the SO_2 loss in the but-2-ene systems is treated as having two components, related to the different SCI.

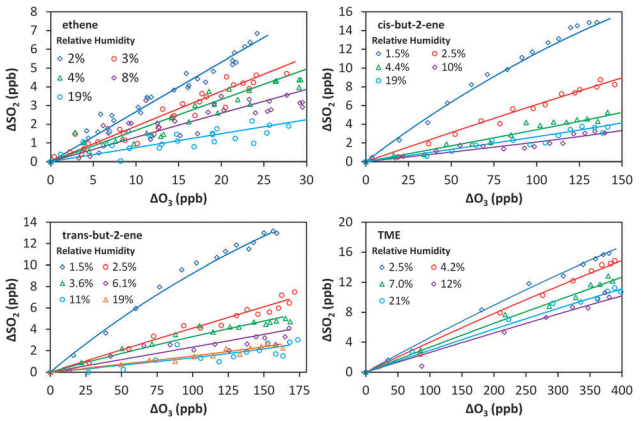

Fig. 1 Cumulative consumption of SO_2 and O_3, ΔSO_2 *versus* ΔO_3, for the ozonolysis of four alkenes in the presence of SO_2 at a range of relative humidities from 1.5–21%. Open symbols are experimental data, corrected for chamber dilution. Solid lines are smoothed fits to the experimental data.

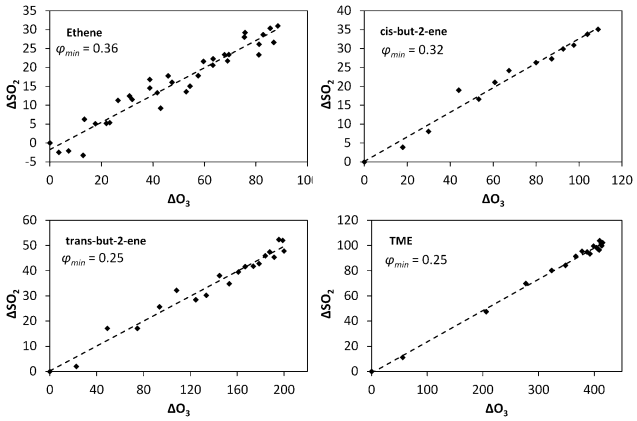

Fig. 2 ΔSO_2 *vs.* ΔO_3 during the excess SO_2 experiments, to determine the minimum SCI yield for the four alkenes.

3. Results and discussion

3.1 Introduction

Table 1 shows the resulting SCI yields obtained for the ozonolysis of ethene, *cis*-but-2-ene, *trans*-but-2-ene and tetramethylethylene (TME); uncertainties are $\pm 2\sigma$, and represent the combined systematic (estimated measurement uncertainty) and precision components. Also shown are past literature values, obtained under various conditions using a range of different SCI scavengers.

The yield of CH_2OO from ethene ozonolysis obtained in this work is 0.37 (±0.04). This yield has been investigated in many previous studies, with values ranging from 0.34–0.50 determined – a more detailed review is available elsewhere.[31] The yield obtained in this work is at the lower end of but within the envelope of these estimates, and is in excellent agreement with the current IUPAC recommendation of 0.37.

The yield of CH_3CHOO from *cis*-but-2-ene ozonolysis obtained in this work is 0.38 (±0.05), with that from *trans*-but-2-ene being 0.28 (±0.03). These values fall within the range of reported literature values of 0.18–0.43 and 0.13–0.53 for *cis*-but-2-ene and *trans*-but-2-ene respectively (Table 1). *cis* and *trans*-but-2-ene both yield (differing) mixtures of *syn* and *anti* conformers of CH_3CHOO, the relative amounts of which are not well known, and which are treated here initially as a single SCI species (this approximation is discussed further in Section 3.3). Berndt *et al.*[32] recently reported a yield of 0.49 (±0.22) for the CH_3CHOO produced from *trans*-but-2-ene ozonolysis (also treating both *syn* and *anti* conformers as a single SCI species).

The yield of $(CH_3)_2COO$ from TME ozonolysis obtained in this work is 0.32 (±0.02). This again falls within the (wide) range in the literature of 0.10–0.65, with Berndt *et al.*[32] most recently reporting a yield of 0.45 (±0.20).

Open Access Article. Published on 06 January 2015. Downloaded on 5/6/2026 12:57:53 PM.
This article is licensed under a Creative Commons Attribution 3.0 Unported Licence.

Table 1 SCI yields derived in this work and reported in the literature. Uncertainty ranges ($\pm 2\sigma$, parentheses) indicate combined precision and systematic measurement error components for this work, and are given as stated for literature studies. All referenced studies were conducted between 700 and 760 Torr. C2B – derived from *cis*-but-2-ene; T2B – derived from *trans*-but-2-ene

SCI	φ_{SCI}	Ref.
CH_2OO	0.37 ($\pm$0.04)	This work
	0.37	MCMv3.2[a] (IUPAC)[33]
	0.35 ($\pm$0.05)	Niki *et al.*[34]
	0.39 ($\pm$0.053)	Hatakeyama *et al.*[35]
	0.47 ($\pm$0.05)	Horie and Moortgat[36]
	0.50 ($\pm$0.04)	Neeb *et al.*[37]
	0.39 ($\pm$0.11)	Hasson *et al.*[38]
	0.54 ($\pm$0.15)	Alam *et al.*[31]
CH_3CHOO (C2B)	0.38 ($\pm$0.05)	This work
	0.19	Rickard *et al.*[39]
	0.18	Niki *et al.*[40]
	0.43	Cox and Penkett[41]
CH_3CHOO (T2B)	0.28 ($\pm$0.03)	This work
	0.49 ($\pm$0.22)	Berndt *et al.*[32]
	0.53 ($\pm$0.24)	Berndt *et al.*[19]
	0.45	Cox and Penkett[41]
	0.19 ($\pm$0.03)	Hatakeyama *et al.*[35]
	0.42	Horie and Moortgat[36]
	0.24 ($\pm$0.07)	Hasson *et al.*[38]
	0.13	Rickard *et al.*[39]
$(CH_3)_2COO$	0.32 ($\pm$0.02)	This work
	0.45 ($\pm$0.20)	Berndt *et al.*[32]
	0.62 ($\pm$0.28)	Berndt *et al.*[19]
	ca. 0.65[b]	Drozd *et al.*[10]
	0.10 ($\pm$0.03)	Hasson *et al.*[38]
	0.30	Niki *et al.*[40]
	0.11	Rickard *et al.*[39]

[a] http://mcm.leeds.ac.uk/MCM/. [b] At 700–760 Torr (low pressure limit of 0.15 at 0 Torr).

Fig. 1 shows the cumulative consumption of SO_2 relative to that of O_3, ΔSO_2 *versus* ΔO_3 (after correction for dilution), as a function of $[H_2O]$ for each experiment for the four alkenes studied. A fit to each experiment, extrapolating the experimental data to evaluate dSO_2/dO_3 at $t = 0$ (start of each experimental run) for use in eqn (E1)–(E3), is also shown. The overall change in SO_2, ΔSO_2, is seen to decrease substantially with increasing humidity (over a relatively narrow range of RH (1.5–20%)) for all four alkenes. This trend would be expected from the understood chemistry ((R1)–(R4)), as there is competition between SO_2, H_2O, and decomposition for reaction with the SCI.

Fig. 3 shows a fit of eqn (E3) to the data for each alkene, giving a slope of k_3/k_2, and an intercept of $(k_d + L)/k_2$. The results appear to show a generally linear relationship; however, for *cis*- and *trans*-but-2-ene and TME, the data point at the highest relative humidity accessible in this work ($[H_2O] = 1.5–2.0 \times 10^{17}$ cm^{-3}) appears to deviate from this relationship. These data points lie outside the 95% confidence intervals defined by all the other (lower relative humidity) data for each alkene. For the analysis to determine k_3/k_2 and $(k_d + L)/k_2$ presented in Table 2, the points at the highest RH are excluded and the kinetic parameters are derived from a linear fit to the measurements from all other experiments. Extended analyses to account for the non-linearity

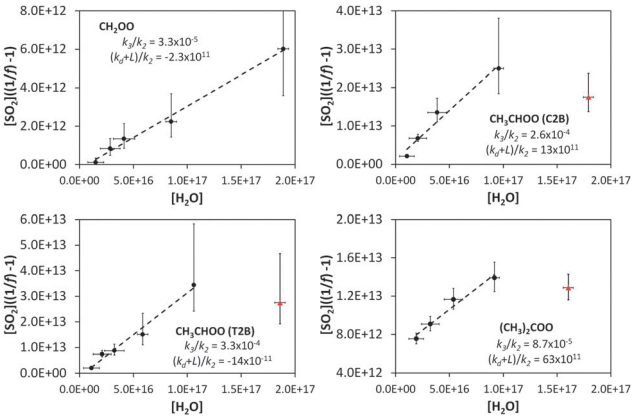

Fig. 3 Application of eqn (E3) to derive rate constants for reaction of CH_2OO, CH_3CHOO (derived from *cis*-but-2-ene; C2B), CH_3CHOO (derived from *trans*-but-2-ene; T2B), and $(CH_3)_2COO$ with H_2O (k_3) and decomposition (k_d), relative to that for reaction with SO_2, k_3/k_2 and $(k_d + L)/k_2$ – see text.

Table 2 SCI relative rate constants derived in this work using the single-SCI water monomer approach (*i.e.* eqn (E3); see text). Uncertainty ranges ($\pm 2\sigma$, parentheses) indicate combined precision and systematic measurement error components

SCI	10^5 k_3/k_2	10^{-11} cm^{-3} k_d/k_2
CH_2OO	3.3 ($\pm$1.1)	−2.3 ($\pm$3.5)
CH_3CHOO (C2B)	26 ($\pm$10)	13 ($\pm$43)
CH_3CHOO (T2B)	33 ($\pm$10)	−14 ($\pm$31)
$(CH_3)_2COO$	8.7 ($\pm$2.5)	63 ($\pm$14)

observed for CH_3CHOO and $(CH_3)_2COO$ are presented in the following sections.

One potential explanation for the observed curvature in the CH_3CHOO and $(CH_3)_2COO$ data is measurement error. ΔSO_2 is relatively small at high $[H_2O]$ compared to the precision of the measurements; however, even allowing for associated uncertainties, the points at high RH do not fit the linear relationship successfully applied to the remaining data points. Moreover, any systematic error in the measurement of O_3, SO_2 or H_2O would also be expected to affect the results for the ethene system (and to a greater extent, given the slow ethene–ozone reaction rate and consequent lower overall chemical SO_2 loss observed), suggesting that the cause lies in contrasting chemical behaviour. In terms of experimental factors, H_2O was measured using multiple approaches (two dew-point hygrometers in addition to a solid state probe) with no evidence for any divergence with RH. SO_2 monitors can exhibit humidity-dependent interferences (quenching of the SO_2 signal), commonly of the order of a few percent, observed at very high RH, and corrected through incorporation of a nafion dryer (fitted in this case); in addition the monitor-derived SO_2 concentration increments were in agreement with those calculated from the measured SO_2 addition and chamber volume, across the relative humidity range studied.

It should be noted that the k_d values reported here represent upper limits, as a consequence of possible further chemical losses for the SCI within our experimental system (as represented by L in eqn (E3), notwithstanding the approach of extrapolating to the start of each experiment to minimise these). Other potential

Open Access Article. Published on 06 January 2015. Downloaded on 5/6/2026 12:57:53 PM.
This article is licensed under a Creative Commons Attribution 3.0 Unported Licence.

fates for SCIs include reaction with ozone,[42,43] other SCI,[43] carbonyl products,[44] acids,[45] or with the parent alkene[43] itself. Sensitivity analyses indicate that the reaction with ozone could be significant, as predicted by theory[42,43] with a possible contribution of up to 10% of SCI loss for $(CH_3)_2COO$ at 2% RH, while total losses from reaction with SCI (self-reaction), carbonyls and alkenes are calculated to account for <1% of the total SCI loss under the experimental conditions applied.

3.2 CH_2OO

3.2.1 Linear Fit. For CH_2OO a linear fit (*i.e.* using eqn (E3) *vs.* H_2O) describes the observations well (Fig. 3) over the entire $[H_2O]$ range studied (1–20 × 10^{16} molecules per cm^{-3}). This fit gives relative rates k_3/k_2 of 3.3 (±1.1) × 10^{-5} and $(k_d + L)/k_2$ of −2.3 (±3.5) × 10^{11} cm^{-3} (Table 2).

These relative rates can be placed on an absolute basis using absolute measurements of k_2(SCI + SO_2). In Table 3 we apply the absolute k_2 values reported by Welz *et al.*,[15] obtained using direct methods at reduced pressure (4 Torr), to the relative rates shown in Table 2. Using this method, the value obtained for $k_3(CH_2OO + H_2O)$ is 1.3 (±0.4) × 10^{-15} cm^3 s^{-1}. This is consistent with the recent determination by Welz *et al.*,[15] that $k_3 < 4 \times 10^{-15}$ cm^3 s^{-1}, but is (*ca.* 14–50 times) greater than the recent estimates of Ouyang *et al.*[18] (k_3 = 2.5 (±1) × 10^{-17} cm^3 s^{-1}) and Stone *et al.*[17] ($k_3 < 9 \times 10^{-17}$ cm^3 s^{-1}).

The derived $(k_d + L)$ value for CH_2OO using this method is −8.8 (±13) s^{-1}, *i.e.* zero within uncertainty. Theoretical work[22] has predicted $k_d(CH_2OO)$ to be small (~0.3 s^{-1}), in agreement with the experimentally derived value reported here.

3.2.2 CH_2OO + $(H_2O)_2$. Recent experimental work[46] has reported the reaction of CH_2OO with the water dimer, $(H_2O)_2$, (reaction (R5)) to be very fast (1.1 × 10^{-11} cm^3 s^{-1} – assuming k_2 = 3.9 × 10^{-11} cm^3 s^{-1} (ref. 15)), in broad agreement with theoretical predictions,[47] but in contrast to other experimental work.[45]

$$CH_2OO + (H_2O)_2 \xrightarrow{k_5} \text{products} \qquad \text{(R5)}$$

The CH_2OO data from this study appear to be well described by a linear fit under the experimental conditions applied (a fast reaction of CH_2OO with $(H_2O)_2$ would be manifested as a significant upward curvature in Fig. 3). However, this does not mean the results are inconsistent with reaction of CH_2OO with $(H_2O)_2$.

In Fig. 4, eqn (E4) (an expanded version of eqn (E3), including the SCI + $(H_2O)_2$ reaction (R5)) is applied to the data, now expressed in terms of $(H_2O)_2$, calculated for each RH *via* the equilibrium constant.[48]

$$[SO_2]_0\left(\frac{1}{f}-1\right) = \frac{k_3}{k_2}\sqrt{\frac{[(H_2O)_2]}{K_p}} + \frac{k_5}{k_2}[(H_2O)_2] + \frac{k_d}{k_2} \qquad \text{(E4)}$$

The value for k_3/k_2 (water monomer) derived from the fit shown in Fig. 4 is 2.5 (±0.7) × 10^{-5}. It is seen that this value is rather insensitive to the inclusion of the $(H_2O)_2$ term in eqn (E4) as the value is within the uncertainties of the linear fit to the data presented in Fig. 3 – see also Table 2. Converting this value to an absolute value using the k_2 from Welz *et al.*[15] gives k_3 = 9.9 (±2.9) × 10^{-16} cm^3 s^{-1}. The derived value of k_d/k_2 is −6.4 (±66) × 10^{10} cm^{-3}, which, using the Welz *et al.*[15] k_2 gives an absolute value for k_d of −1.5 (±16) s^{-1}. This is again indistinguishable from zero, within uncertainty, as is the k_d determined from eqn (E3) (Fig. 3). Note the large uncertainties in k_d, resulting from allowing three parameters to vary in the optimisation; consequently k_d was fixed to zero in eqn (E4) to determine the k_3/k_2 and k_5/k_2 values.

The resulting value of k_5/k_2 (water dimer) is 1.4 (±1.8) × 10^{-2}. Converting this to an absolute value using the k_2 from Welz *et al.*[15] gives k_5 = 5.6 (±7.0) × 10^{-13} cm^3 s^{-1}. This is roughly a factor of twenty smaller than the value derived by Berndt *et al.*,[46] but within a factor of two of the upper limit for k_5 deduced by Welz *et al.* (<3 × 10^{-13} cm^3 s^{-1}) (ref. 45) from the data presented by Stone *et al.*[17] The inset plot in Fig. 4 also shows two additional fits generated using eqn (E4) with k_3/k_2 fixed to 9.9 × 10^{-16} and k_d fixed to zero. One fit line uses the k_5 value reported by Berndt *et al.*[46] (blue dashed line). This is seen to overestimate the presented data. The green dotted line shows a fit to the upper limits of the uncertainties of the measured data. This yields a k_5/k_2 value of 0.10 (±0.01), giving an upper limit k_5 value of 3.9 (±0.39) × 10^{-12} cm^3 s^{-1}.

Table 3 Comparison of SCI relative rate constants derived in this work to relative and absolute values from the literature. Uncertainty ranges (±2σ) indicate combined precision and systematic measurement error components

SCI	10^5 k_3/k_2	10^{15} k_3 (cm^3 s^{-1})	10^{-11} k_d/k_2 (cm^{-3})	k_d (s^{-1})	Ref.	Method	Conditions[a]
CH_2OO	3.3 (±1.1)	1.3 (±0.4)[b]	−2.3 (±3.5)	−8.8 (±13)[b]	This work	Ethene ozonolysis	298–303 K
		<4			Welz *et al.*[15]	Alkyl iodide photolysis	4 Torr; 298 K
		<0.09			Stone *et al.*[17]	Alkyl iodide photolysis	200 Torr; 295 K
CH_3CHOO	26 (±10)	12 (±4.5)[c]	13 (±43)	59 (±196)[c]	This work	C2B ozonolysis	296–302 K
	33 (±10)	15 (±4.5)[c]	−14 (±31)	−64 (±141)[c]	This work	T2B ozonolysis	297–302 K
		anti 10 (±4); *syn* <4			Taatjes *et al.*[16]	Alkyl iodide photolysis	4 Torr; 298 K
	8.8 (±0.4)		12 (±0.1)		Berndt *et al.*[32]	T2B ozonolysis	293 K
				76 (25–228)	Fenske *et al.*[26]	T2B ozonolysis	296 K
$(CH_3)_2COO$	8.7 (±2.5)	2.1 (±0.6)[d]	63 (±14)	151 (±35)[d]	This work	TME ozonolysis	298–299 K
	<0.4		42 (±3)		Berndt *et al.*[32]	TME ozonolysis	293 K

[a] Experiments were conducted at atmospheric pressure unless stated otherwise. [b] Assuming k_2 = 3.9 × 10^{-11} cm^3 s^{-1} (Welz *et al.*[15]). [c] Assuming k_2 = 4.55 × 10^{-11} cm^3 s^{-1}. Average of k_2 for *syn* and *anti* CH_3CHOO conformers from Taatjes *et al.*[16] [d] Assuming k_2 = 2.4 × 10^{-11} cm^3 s^{-1}. k_2 for *syn*-CH_3CHOO from Taatjes *et al.*[16]

Open Access Article. Published on 06 January 2015. Downloaded on 5/6/2026 12:57:53 PM.
This article is licensed under a Creative Commons Attribution 3.0 Unported Licence.

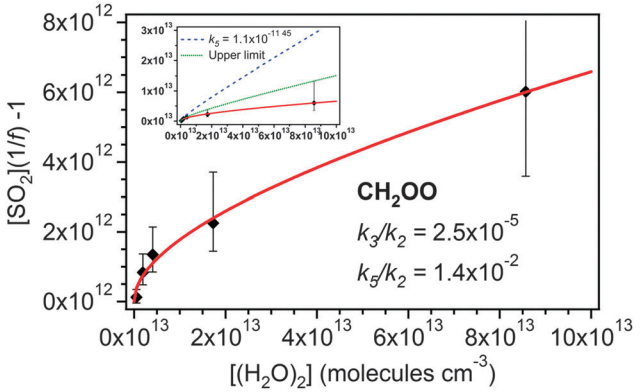

Fig. 4 Application of eqn (E4) to derive rate constants for reaction of CH_2OO with H_2O (k_3/k_2) and $(H_2O)_2$ (k_5/k_2) relative to that of CH_2OO with SO_2. Inset: eqn (E4) as shown in the main figure (red line), (E4) applied using the dimer reaction rate (k_5) reported by Berndt *et al.*[45] (1.1×10^{-11} cm^3 s^{-1}) (dashed line) and a fit of (E4) to the upper limits of the uncertainties in the ethene data (solid green line).

The contribution of $(H_2O)_2$ to the removal of CH_2OO increases in relation to that of H_2O as $[H_2O]$ increases. Hence at typical atmospheric $[H_2O]$ ($\sim$2.5–7.5 $\times$ 10^{17} molecules per cm^{-3}), greater than was accessible in this study, reaction with $(H_2O)_2$ could become the dominant sink for CH_2OO. In this case using just the H_2O monomer kinetics in models would considerably underestimate the total effect of water on removal of CH_2OO in the atmosphere.

3.3 CH_3CHOO

3.3.1 Single SCI Approach. The CH_3CHOO data shown in Fig. 3 for both *cis* and *trans*-but-2-ene appear to be well described (within the uncertainties) by a linear fit to eqn (E3), with the exception of the experiment at the highest RH ($[H_2O]$ = 1.8–1.9 $\times$ 10^{17} cm^{-3}) in both cases. The kinetic parameters derived from a linear fit to the data (Fig. 3), using eqn (E3) (which treats the system as producing a single SCI), excluding the highest RH experiments, are shown in Table 2. Very similar results are obtained for k_3/k_2 for CH_3CHOO derived from both *cis*- and *trans*-but-2-ene ozonolysis, with values of 26 ($\pm$10) $\times$ 10^{-5} and 33 ($\pm$10) $\times$ 10^{-5} respectively. The $(k_d + L)/k_2$ obtained for CH_3CHOO from *cis*-but-2-ene ozonolysis is 13 ($\pm$43) $\times$ 10^{11} molecule cm^{-3} and from *trans*-but-2-ene ozonolysis $-$14 ($\pm$31) $\times$ 10^{11} molecule cm^{-3}. Berndt *et al.*[32] reported the k_3/k_2 ratio from *trans*-but-2-ene ozonolysis to be 8.8 ($\pm$0.4) $\times$ 10^{-5} (also assuming a single SCI system), a factor of 3.75 smaller than that reported here.

The relative rate constants (Table 2) can be placed on an absolute basis using the measurements of $k_2(SCI + SO_2)$ reported by Taatjes *et al.*[16] (derived using the same methodology as for CH_2OO) (Table 3). As eqn (E3) treats the SCI produced as a single SCI, we use an average of the *syn* and *anti* conformer rates presented in Taatjes *et al.*,[16] 4.55 $\times$ 10^{-11} cm^3 s^{-1}. Using this method, the value obtained for $k_3(CH_3CHOO + H_2O)$ from *cis*-but-2-ene ozonolysis is 12 ($\pm$4.5) $\times$ 10^{-15} cm^3 s^{-1} and from *trans*-but-2-ene ozonolysis is 15 ($\pm$4.5) $\times$ 10^{-15} cm^3 s^{-1}. Taking a mean of the k_3 values reported for the two CH_3CHOO conformers by Taatjes *et al.*[16] gives a value of 7.0 $\times$ 10^{-15} cm^3 s^{-1}, while Sheps *et al.*[49] give a mean value of 12 $\times$ 10^{-15} cm^3 s^{-1}. The values obtained for $(k_d + L)$ are 59 ($\pm$196) s^{-1} from *cis*-but-2-ene and $-$64 ($\pm$141) s^{-1} from *trans*-but-2-ene. Clearly there is a large uncertainty associated with the k_d determined from this analysis. Fenske *et al.*[26] have reported $k_d(CH_3CHOO)$ from *trans*-but-2-ene ozonolysis to be 76 s^{-1} (accurate to within a factor of three).

3.2.2 Two conformer system. In Fig. 1 it is evident that dSO_2/dO_3 falls rapidly with increasing $[H_2O]$ for all but-2-ene experiments as RH is initially increased, but that the experiments at higher RH all appear to display a similar dSO_2/dO_3, *i.e.* the trend in decreasing SO_2 removal with increasing H_2O levels off. From this observation it appears that there may be competing H_2O dependencies to the SO_2 loss present. This is manifested in Fig. 3 as a curving over of the data at high RH. We propose two possible explanations for this observation: firstly that it arises from differing kinetics of the two CH_3CHOO conformers formed in but-2-ene ozonolysis; secondly that the behaviour may reflect the presence of an additional oxidant being formed in the ozonolysis system that reacts with SO_2 but is less sensitive to H_2O. The first of these possibilities is discussed below, the second is discussed in relation to $(CH_3)_2COO$ in the following section.

One explanation for the observed non-linearity at high RH apparent in Fig. 3 is the differing reactivities of the *syn*- and *anti*-conformers of CH_3CHOO produced in the ozonolysis of *cis*- and *trans*-but-2-ene. It has been predicted[50] that the *anti*-conformer reacts with H_2O several orders of magnitude faster than the *syn*-conformer, while the rate constant for the SCI reaction with SO_2 has been determined experimentally[16] to be about a factor of three greater for the *anti*-conformer than the *syn*-conformer. The fraction of each conformer that is lost to reaction with SO_2 can be considered in the same way as illustrated in eqn (E2), leading to eqn (E5) and (E6) below, plus simplifications outlined in the following text. The total loss of SO_2 to CH_3CHOO is then the sum of the fractional loss to each conformer, multiplied by the relative SCI yield (γ) (*i.e.* φ^{syn}/φ) of that conformer (eqn (E7)).

$$f^{syn} = \frac{[SO_2]}{[SO_2] + \frac{k_3^{syn}}{k_2^{syn}}[H_2O] + \frac{k_d^{syn}}{k_2^{syn}}} \approx \frac{[SO_2]}{[SO_2] + \frac{k_d^{syn}}{k_2^{syn}}} \quad \text{(E5)}$$

$$f^{anti} = \frac{[SO_2]}{[SO_2] + \frac{k_3^{anti}}{k_2^{anti}}[H_2O] + \frac{k_d^{anti}}{k_2^{anti}}} \approx \frac{[SO_2]}{[SO_2] + \frac{k_3^{anti}}{k_2^{anti}}[H_2O]} \quad \text{(E6)}$$

$$f = \gamma^{syn} f^{syn} + \gamma^{anti} f^{anti} \quad \text{(E7)}$$

Eqn (E8) can then be fitted to the data presented in Fig. 3 for *cis*- and *trans*-but-2-ene (Fig. 5).

$$[SO_2]\left(\frac{1}{f} - 1\right) = [SO_2]\left(\frac{1}{\gamma^{syn} f^{syn} + \gamma^{anti} f^{anti}} - 1\right) \quad \text{(E8)}$$

Here we make two assumptions to reduce the degrees of freedom and hence make the problem tractable with the

Open Access Article. Published on 06 January 2015. Downloaded on 5/6/2026 12:57:53 PM.
This article is licensed under a Creative Commons Attribution 3.0 Unported Licence.

dataset available. First it is assumed that $k_3^{syn}[H_2O]$ may be neglected, in keeping with theoretical predictions[24] predicting k_d^{syn} to be over three orders of magnitude greater than $k_3^{syn}[H_2O]$. Further theoretical work[50] predicts a rate constant for *syn*-$CH_3CHOO + H_2O$ of 2.39×10^{-18} cm^3 s^{-1}, and recent experimental work[49] yields an upper limit for k_3^{syn} of $< 2 \times 10^{-16}$ cm^3 s^{-1}. Hence with k_d^{syn} expected to be relatively fast, given the decomposition rate presented here for $(CH_3)_2COO$ (a *syn*-conformer) and the facile decomposition route available *via* the hydroperoxide mechanism for the *syn*-conformer, it can be assumed that $k_d^{syn} \gg k_3^{syn}[H_2O]$ at the experimental conditions reported here. Second it is assumed that $k_d^{anti} \ll k_3^{anti}[H_2O]$ under the experimental conditions used. If the kinetics derived from treating the but-2-ene data in Fig. 3 as representing a single SCI are dominated by the *anti*-conformer then the k_d derived from these kinetics, which is indistinguishable from zero within the uncertainties, suggests that k_d^{anti} is small. Taatjes *et al.*[16] report k_3^{anti} to be 1.0 ($\pm$0.4) $\times 10^{-14}$ cm^3 s^{-1}, while Sheps *et al.*[49] report a value of 2.4 ($\pm$0.4) $\times 10^{-14}$ cm^3 s^{-1}. Thus, even at the lowest $[H_2O]$ considered here ($\sim 1 \times 10^{16}$ cm^{-3}), loss of *anti*-CH_3CHOO to H_2O would be >100 s^{-1}, and decomposition negligible in comparison (including a k_d^{anti} of 50 s^{-1} changes the derived k_3^{anti} and k_d^{syn} values by $<5\%$).

Fitting eqn (E8) to the data shown in Fig. 5 derives a range of values for k_3^{anti} and k_d^{syn} dependent on the values of γ^{anti} and γ^{syn} used. As the CIs, once formed and thermalised, are expected to show the same kinetic behaviour in these experiments irrespective of their precursor alkene, the measurements from the *cis*-but-2-ene and *trans*-but-2-ene experiments can be used in combination to constrain k_3^{anti}, k_d^{syn} and also γ^{syn} and γ^{anti} from each alkene. Fig. 6 plots the k_3^{anti} *vs.* k_d^{syn} determined at different γ^{syn} and γ^{anti} from *cis*-but-2-ene and *trans*-but-2-ene. Where these two lines intercept represents the unique solution for both k_3^{anti} and k_d^{syn} and for γ^{syn} and γ^{anti} (Table 4).

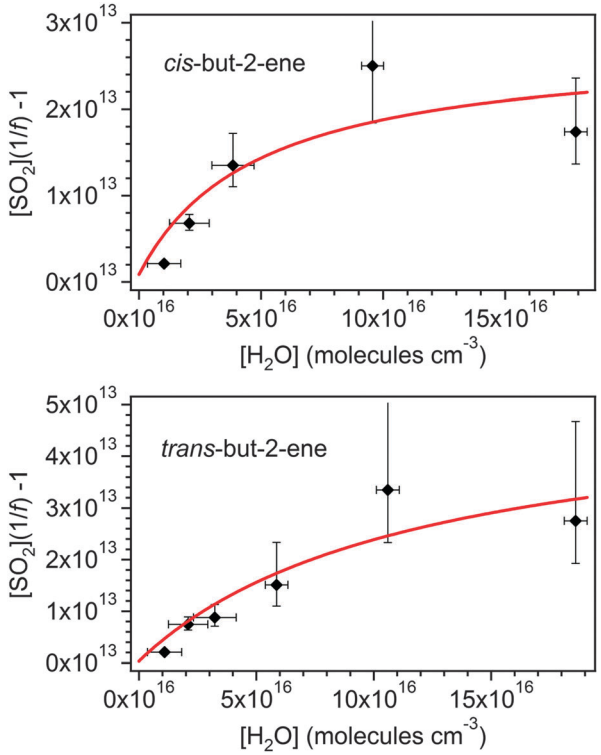

Fig. 5 Fits of eqn (E8) to the *cis*-but-2-ene and *trans*-but-2-ene data shown in Fig. 3. γ^{syn} and γ^{anti} are 0.45 and 0.55 for *cis*-but-2-ene and 0.25 and 0.75 for *trans*-but-2-ene (see Fig. 6).

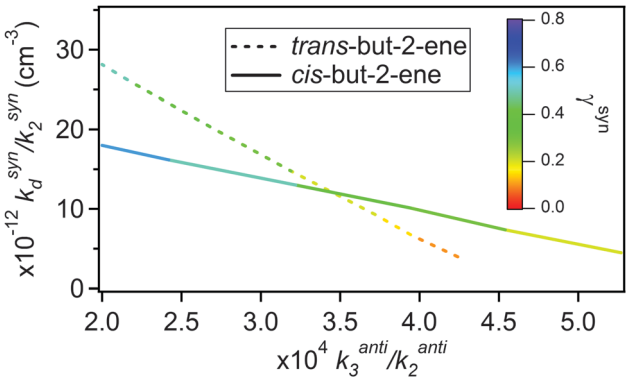

Fig. 6 The ranges of k_3^{anti}/k_2^{anti} and k_d^{syn}/k_2^{syn} determined from fitting eqn (E8) to the but-2-ene data (Fig. 5). The colour legend shows the fraction of the total CH_3CHOO formed that is *syn*-CH_3CHOO (γ^{syn}).

Fig. 4 also determines the relative yields of the two conformers, γ^{syn} and γ^{anti} (which in turn has been used to derive the optimised fits shown in Fig. 5). For *cis*-but-2-ene these are determined as 0.45 and 0.55 for γ^{syn} and γ^{anti} respectively. For *trans*-but-2-ene they are determined as 0.25 for γ^{syn} and 0.75 for γ^{anti}. The analysis performed in this section has implications for the determination of the SCI yield. Using the relative rate constant k_3/k_2(*anti*-CH_3CHOO) obtained, as shown in Table 4, it is calculated that $\sim$90% of the *anti*-CH_3CHOO produced in the SCI yield experiments would react with SO_2. From the determined k_d/k_2(*syn*-CH_3CHOO) it is calculated that $\sim$67% of the *syn*-CH_3CHOO produced in the SCI yield experiments would react with SO_2. Applying these (with the corresponding *syn* and *anti* yields shown in Table 4) corrections to φ_{min} determines total SCI yields of 0.29 for *trans*-but-2-ene and 0.42 for *cis*-but-2-ene. These values both lie within the uncertainties in the SCI yields presented in Table 1 for the two but-2-ene systems.

It is not practicable to assess the possible contribution of the water dimer to the SCI loss for CH_3CHOO because of the

Table 4 Kinetic parameters derived for *syn*-CH_3CHOO and *anti*-CH_3CHOO from two-component fits to the *trans*-but-2-ene (T2B) and *cis*-but-2-ene (C2B) experiments (see Fig. 5). Also relative (γ) and absolute (φ) yields of the two conformers

					γ^a		φ			
CH_3CHOO	$10^4\ k_3/k_2$	$10^{14}\ k_3$ ($cm^3\ s^{-1}$)	$10^{-13}\ k_d/k_2$ (cm^{-3})	k_d (s^{-1})	T2B	C2B	T2B	C2B	Ref.	Conditions[b]
syn	—	—	1.2 (±1.1)	288 (±275)	0.25	0.45	0.07	0.17	This work	—
		<0.4							Taatjes *et al.*[16]	4 Torr
		<0.02							Sheps *et al.*[49]	200 Torr
				20 (3–30)					Novelli *et al.*[23]	735 Torr
anti	3.5 (±3.1)	2.3 (±2.1)	—	—	0.75	0.55	0.21	0.21	This work	—
		1.0 (±0.4)							Taatjes *et al.*[16]	4 Torr
		2.4 (±0.4)							Sheps *et al.*[49]	200 Torr

[a] $\gamma^{syn} = \varphi^{syn}/\varphi$. [b] Experiments were conducted at atmospheric pressure unless stated otherwise and temperatures from 293 to 303 K.

Open Access Article. Published on 06 January 2015. Downloaded on 5/6/2026 12:57:53 PM. This article is licensed under a Creative Commons Attribution 3.0 Unported Licence.

number of free parameters that would result for a small dataset. However, theoretical predictions[47] suggest that this may be less important for CH_3CHOO than for CH_2OO, indicating $k(H_2O)_2/k(H_2O)$ to be two orders of magnitude smaller for *anti*-CH_3CHOO than for CH_2OO.

3.4 $(CH_3)_2COO$

3.4.1 Linear fit. For $(CH_3)_2COO$ a value of 8.7 (±2.5) × 10^{-5} (Table 2) was obtained from a linear fit to the data in Fig. 3, excluding the experiment performed at the highest RH ($[H_2O]$ = 1.6 × 10^{17} cm^{-3}) from the regression. $(k_d + L)/k_2$ for $(CH_3)_2COO$ was determined as 63 (±14) × 10^{11} molecule per cm^{-3}. These values can be placed on an absolute basis using the measurements of k_2(*syn*-$CH_3CHOO + SO_2$) reported by Taatjes *et al.*[16] as there are no reported k_2 values for $(CH_3)_2CHOO$ from direct experiments and $(CH_3)_2COO$ is a *syn*-conformer (*i.e.* there is always a methyl group in a *syn* orientation to the terminal oxygen). This gives values for k_3 ($(CH_3)_2COO + H_2O$) of 2.1 (±0.6) × 10^{-15} $cm^3\ s^{-1}$ and for k_d of 151 (±35) s^{-1} (Table 3).

Berndt *et al.*[32] have recently reported the k_3/k_2 ratio for $(CH_3)_2COO$ to be $<0.4 \times 10^{-5}$ (*i.e.* approximately a factor of 22 lower than the relative rate reported in this study). Theoretical predictions[50] also suggest k_3 to be very slow, 3.9 × 10^{-17} $cm^3\ s^{-1}$. No measured values have been reported for k_d ($(CH_3)_2COO$), but a more facile overall decomposition than for CH_2OO or the mean of the CH_3CHOO isomers might be anticipated as the vinyl-hydroperoxide isomerisation channel[26] is always available.

3.4.2 Additional oxidant. In the case of the SCI formed from TME ozonolysis, $(CH_3)_2COO$, there is always a methyl group in a *syn* position to the carbonyl oxide moiety, thus the analysis presented in Section 3.3.2 for the CH_3CHOO isomers does not apply. A possible alternative explanation for the observed behaviour (and possible contributor to the behaviour observed in the but-2-ene systems) is that there is a further oxidant (X) of SO_2, in addition to the SCI, being formed during the ozonolysis reaction. If this oxidant reacts relatively slowly with H_2O, it could give rise to the apparent 'two component' nature of the observations seen in Fig. 3. It may also provide an alternative explanation of the observed nature of the SO_2 loss from the but-2-ene experiments or could be occurring in addition to the effects of differing conformer reactivities.

Eqn (E9) (below) is an expanded version of (E2), in which we consider the contribution from a second SO_2 oxidant, making the approximation that this species does not react appreciably with water vapour. In eqn (E9), f is the sum of f^{SCI} (the fraction of SCI reacting with SO_2) and f^x, each multiplied by the relative yield of the total oxidant (*i.e.* SCI + X) γ^{SCI} and γ^x. Following the assumption of negligible H_2O reactivity, $(dSO_2/dO_3)_x$ in eqn (E9) can be derived from the SO_2 loss at the highest RH experiments (*i.e.* when all the SO_2 loss is attributed to X + SO_2) of ~10 ppbv. Therefore, loss of SO_2 from reaction with X, relative to the loss of O_3 $(dSO_2/dO_3)_x$ is approximately 0.025. φ represents the total oxidant yield (*i.e.* $\varphi_{SCI} + \varphi_x$). Assuming that γ^x is not dominant (<0.5), then φ, as calculated from correcting φ_{min} as in Section 3.1, changes little (0.31–0.34) from the value presented in Table 1. Eqn (E10) is then an expanded version of eqn (E3) that includes the additional oxidant term.

$$f = \gamma^{SCI} f^{SCI} + \gamma^x f^x = \gamma^{SCI} f^{SCI} + \frac{1}{\phi}\left(\frac{dSO_2}{dO_3}\right)_x \quad \text{(E9)}$$

$$[SO_2]\left(\frac{1}{f} - 1\right) = [SO_2]\left[\left(\frac{\gamma^{SCI}[SO_2]}{[SO_2] + \frac{k_3}{k_2}[H_2O] + \frac{k_d}{k_2}} + \frac{1}{\phi}\left(\frac{dSO_2}{dO_3}\right)_x\right)^{-1} - 1\right] \quad \text{(E10)}$$

Fig. 7 shows eqn (E10) fitted to the TME data from Fig. 3. It is not possible to determine unique values for the parameters included in eqn (E10) due to the degrees of freedom *vs.* the limited data set. The fit shown in Fig. 7 uses values of φ = 0.34, γ^{SCI} = 0.88, k_3/k_2 = 6.7 × 10^{-4} and k_d/k_2 = 1.2 × 10^{12} cm^{-3}. However, Fig. 7 does demonstrate that a two-oxidant system, as represented by eqn (E10), is able to describe the data within uncertainty.

Fig. 7 also includes a linear fit (*i.e.* eqn (E3)) to the full $(CH_3)_2COO$ dataset (including the highest RH experiment). While it seems unlikely that the curvature observed in the data is a result of measurement error (as described in Section 3.1), this must be considered as a possibility for $(CH_3)_2COO$ in light of the two conformer explanation not being applicable. The linear fit in Fig. 7 gives a k_3/k_2 value of 3.8 (±3.2) × 10^{-5} $cm^3\ s^{-1}$, a factor of two smaller than the k_3/k_2 value presented in Table 2.

Open Access Article. Published on 06 January 2015. Downloaded on 5/6/2026 12:57:53 PM.
This article is licensed under a Creative Commons Attribution 3.0 Unported Licence.

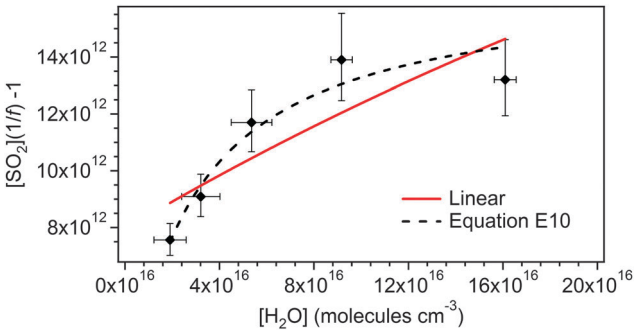

Fig. 7 Data for TME ozonolysis (as shown in Fig. 3), with fit to eqn (E10), and linear fit to the full dataset.

The most obvious candidate for an additional oxidant present to consume SO_2 is OH. OH radicals are produced in the chamber, primarily (in the absence of sunlight and NO_x) through the alkene + ozone reaction.[11] However cyclohexane was added in excess at the beginning of each experiment to act as an OH scavenger, such that SO_2 reaction with OH was calculated to be $\leq$1% of the total chemical SO_2 removal in all experiments. Other potential candidates for this oxidant species include the (stabilised) vinyl hydroperoxide (VHP) intermediate, a secondary ozonide (formed through an SO_2–SCI cyclic adduct), and dioxirane (Scheme 1).

Drozd *et al.*[10] have presented evidence for substantial VHP stabilisation (derived from the $(CH_3)_2COO$ CI) at pressures of a few hundred Torr, with a lifetime of the order of a few hundred milliseconds with respect to decomposition to form OH, providing scope for bimolecular reactions of this species to occur. This would be consistent with the kinetic observations presented here: a small yield in the systems with *syn*-SCIs, while for ethene, no VHP intermediate is available, and the standard chemistry ((R1)–(R4)) can be used to satisfactorily reproduce the observations. However, no significant SO_2 reactivity is known for the peroxide or alkene functionalities present in the closed shell VHP in isolation, hence it may be surprising if this species reacted rapidly with SO_2, although theoretical studies have suggested that the VHP may react with H_2O.[23]

Secondary ozonide species, formed as an adduct from the SCI + SO_2 reaction, have been suggested to account for the observed isotopic exchange in alkene–ozone–SO_2 systems,[25] and are suggested to have lifetimes of seconds or longer.[19] Such a secondary ozonide could react with a further SO_2 molecule (*i.e.* a two-component secondary ozonide catalysed oxidation route for SO_2 to SO_3 conversion), however a substantial humidity dependence to the overall process may still be anticipated (on the basis of SCI removal through the SCI + H_2O reaction), which is not observed here.

The 'hot acid/ester channel' (rearrangement and decomposition *via* a dioxirane intermediate) is the dominant isomerisation route available for *anti*-SCIs. Although the hydroperoxide channel is the principal isomerisation route for *syn*-SCIs, the ester mechanism is also available,[25] and it is likely that a small proportion of the *syn*-CI will isomerise through this channel to form a dioxirane. Dioxiranes are known to be highly reactive and selective oxidising agents,[51,52] and have a particular affinity for sulphur compounds.[53] Additional oxidation of SO_2 by the dioxirane, over and above that arising directly from reaction with the SCI, could then explain the observed behaviour of SO_2 in the TME experiments (and contribute to the behaviour observed for the but-2-ene systems). For the small CI CH_2OO, formed in the ethene system, it has been predicted that the dioxirane formed is considerably less stable than the methyl substituted dioxiranes formed from but-2-ene and TME ozonolysis, and furthermore will decompose promptly due to chemical activation.

The possibility of non-CI products of the ozonolysis system being responsible for some of the observed SO_2 oxidation has been suggested previously as an alternative (or additional) explanation for the observed behaviour of SO_2 in the atmosphere.[1,54,55] In their laboratory study Berndt *et al.*[19] note that their data were not perfectly described by a model in which a single (SCI related) SO_2 oxidation process was assumed, and commented that the SO_2 oxidation in ozonolysis systems may in fact be more complex. Taatjes *et al.*[56] have recently suggested that these data[19] are consistent with a two-component oxidation system, either two processes removing SO_2 in parallel (as described above), or through a sequential two-step SO_2 removal mechanism, such as the secondary ozonide route outlined above. However, this latter mechanism cannot (in isolation) account for the observations presented here.

The presence of an additional oxidant would have implications for the role of alkene ozonolysis in oxidation of trace gases in the atmosphere. If an oxidant is being formed that reacts slowly with H_2O then this, perhaps in addition to SCI, may contribute to the additional (non-OH) SO_2 oxidation observed in recent field experiments.[1] Further investigation of this possibility is needed.

As for CH_3CHOO, the analysis performed in this section has implications for the determination of the SCI ($(CH_3)_2COO$) yield. Using the value of k_d derived from the linear fit to all the data shown in Fig. 7 would indicate an SCI yield of 0.33. Using the value of k_d derived from the 'additional oxidant fit in Fig. 7, and taking into account that $\sim$10 ppb of the SO_2 loss in the high SO_2 experiment would be attributed to reaction with the additional oxidant rather than the SCI, determines a slightly lower φ_{min} of 0.23, and a corrected yield of 0.32, very similar to that shown in Table 1. Both of these possible alternative SCI yields lie within the uncertainties in the SCI yield from TME ozonolysis presented in Table 1.

As for CH_3CHOO, it is not possible to quantitatively consider the contribution of the water dimer to the SCI loss given the limited data, but theory[53] predicts $k(H_2O)_2/k(H_2O)$ to be three orders of magnitude smaller than that for CH_2OO suggesting that reaction with the water dimer would be unimportant for $(CH_3)_2COO$ at typical atmospheric boundary layer $[H_2O]$.

4. Atmospheric implications

The derived values for k_3 reported in Table 3 correspond to loss rates for reaction of SCI with H_2O in the atmosphere of 650 s^{-1} for CH_2OO, $\sim$3500 s^{-1} for CH_3CHOO and $\sim$1050 s^{-1} for $(CH_3)_2COO$

Open Access Article. Published on 06 January 2015. Downloaded on 5/6/2026 12:57:53 PM.
This article is licensed under a Creative Commons Attribution 3.0 Unported Licence.

(assuming $[H_2O] = 5 \times 10^{17}$ molecules per cm^{-3}, equivalent to an RH of 65% at 298 K). Comparing this to the derived k_d values it is seen that reaction with H_2O is predicted to be the main sink for SCI in the atmosphere, but also that loss through decomposition cannot be neglected for some SCIs – contributing on the order of 0–1% for CH_3CHOO and 13% for $(CH_3)_2COO$.

An estimate of a mean steady state SCI concentration in the background atmospheric boundary layer can then be calculated using eqn (E11).

$$[SCI] = \frac{[Alkene][O_3]k_1\phi}{k_3[H_2O] + k_d} \quad (E11)$$

Using the data given below, a steady state SCI concentration of 1.7×10^3 molecules per cm^{-3} is estimated for an ozonolysis source (noting that other potential atmospheric sources of SCI exist, *e.g.* photolysis of alkyl-iodides in the marine boundary layer, and sinks, *e.g.* reaction with NO and NO_2). This assumes an ozone mixing ratio of 40 ppbv, an alkene mixing ratio of 2 ppbv, φ of 0.35, and mean reaction rate constants k_1 (alkene–ozone) of 1×10^{-16} cm^3 s^{-1}; k_2 (SCI + SO_2) of 3.5×10^{-11} cm^3 s^{-1}, k_3 (SCI + H_2O) of 2×10^{-15} cm^3 s^{-1}, k_d of 30 s^{-1} with $[H_2O]$ of 5×10^{17} cm^{-3} (RH $\sim$ 65%).

However, in the case of CH_3CHOO the data shown in Fig. 3, and the discussion above, indicate contributions from multiple species – *syn*- and *anti*-conformers with contrasting behaviour. It is clear that the burden of CH_3CHOO in the atmosphere would be better described by considering these two fractions of SO_2 loss separately. Eqn (E12) expands eqn (E11) to treat the two conformers separately, where [SCI] = [*anti*-SCI] + [*syn*-SCI], making the same assumptions as for the analysis of CH_3CHOO in eqn (E5) and (E6). k_3^{anti} is estimated to be 1×10^{-14} cm^3 s^{-1} (taking into account that CH_2OO is considered as an *anti*-SCI in this analysis and that the derived $k_3(CH_2OO)$ is more than an order of magnitude smaller than the derived $k_3(CH_3CHOO)$ of 2.3×10^{-14} cm^3 s^{-1}), k_d^{syn} is assumed to be 200 s^{-1} and $\varphi^{anti} = \varphi^{syn} = 0.175$. Additionally the *anti*-SCI + water dimer reaction is also considered, using a value of 5.6×10^{-13} cm^3 s^{-1} as derived for CH_2OO in this work.

$$[SCI] = [Alkene][O_3]k_1\left(\frac{\phi^{anti}}{k_3^{anti}[H_2O] + k_5^{anti}K_p[H_2O]^2} + \frac{\phi^{syn}}{k_d^{syn}}\right) \quad (E12)$$

Using these values in eqn (E12) determines [*anti*-SCI] = 164 molecules per cm^{-3} and [*syn*-SCI] = 4.4×10^3 molecules per cm^{-3}. The formation of an additional oxidant during alkene ozonolysis would be expected to have a similar effect to the two component contribution presented in eqn (E12) based on the apparent yields from the experiments presented here. From this analysis the atmospheric SCI burden is seen to likely be dominated by *syn*-SCI since this term is at least an order of magnitude greater than the *anti*-SCI term.

A typical diurnal loss rate of SO_2 to OH ($k_{OH} \times [OH]$) is 9×10^{-7} s^{-1},[15] while the SO_2 loss rate due to reaction with SCI, using the values derived from eqn (E12), would be 1.2×10^{-7} s^{-1}. This suggests, for the conditions and assumptions given above, the loss of SO_2 to SCI to be about 13% of loss to OH. This analysis neglects additional chemical sinks for SCI, which would reduce SCI abundance but are unlikely to be competitive with the two main SCI loss processes identified herein. SCI concentrations are expected to vary greatly depending on the local environment, *e.g.* alkene abundance may be considerably higher (and with a different reactive mix of alkenes) in a forested environment, compared to a rural background environment. The majority of the SCI burden, particularly in forested regions, is likely to be dominated by larger SCI derived from (C_5) isoprene and (C_{10}) monoterpenes. The chemistry of these species could differ greatly from the small SCI reported here (which we have found to be structure specific, even for small alkene systems), especially for tethered SCI derived from ozonolysis of internal double bonds within (for example) some monoterpenes. It is clear that the total SCI loss rate is dependent upon SCI identity and configuration, and that further work is required to quantify speciated SCI in the atmosphere, and to accurately calculate SCI concentrations for use in atmospheric modelling.

5. Conclusions

It has been shown that at relatively low $[H_2O]$ ($< 1 \times 10^{17}$ cm^{-3}) the loss of SO_2 in the presence of four ozone–alkene systems: ethene, *cis*-but-2-ene, *trans*-but-2-ene and 2,3-dimethyl-but-2-ene significantly decreases with increasing water vapour. This is consistent with production of a stabilised Criegee intermediate from the ozonolysis reaction and subsequent reaction of this species with SO_2 and H_2O. Competition between H_2O and SO_2 for reaction with the SCI leads to the observed relationship which is sensitive to water vapour abundance over a relatively narrow range of RH. Derived kinetic data for these ozonolysis systems shows that the reaction rates are dependent on the structure of the SCI. At $[H_2O] > 1 \times 10^{17}$ cm^{-3} the SO_2 loss in the presence of *cis*- and *trans*-but-2-ene, and 2,3-dimethyl-but-2-ene appears to show a reduced dependence upon H_2O. The results suggest that there is an H_2O dependent and an H_2O independent fraction to the observed SO_2 loss in these systems. These two fractions may be attributable to differing kinetics of the two conformers produced in but-2-ene ozonolysis or to other oxidant products of the alkene ozonolysis reaction. This observation means that SCI structure must be considered in atmospheric modelling of SCI production from alkene ozonolysis, and suggests that the atmospheric SCI burden (and hence the oxidation of trace gases) will be dominated by *syn*-SCI.

This work provides constraints on the behaviour of SCI formed through alkene ozonolysis under conditions relevant to the atmospheric boundary layer, but also highlights the complex nature and incomplete current understanding of the ozonolysis system. Further research is needed to definitively quantify the impact of this chemistry upon atmospheric oxidation.

Acknowledgements

The assistance of the EUPHORE staff is gratefully acknowledged. Marie Camredon, Stephanie La and Mat Evans are thanked for

helpful discussions. This work was funded by EU FP7 EUROCHAMP 2 Transnational Access activity (E2-2012-05-28-0077), the UK NERC (NE/K005448/1) and Fundacion CEAM. Fundación CEAM is partly supported by Generalitat Valenciana, and the projects GRACCIE (Consolider-Ingenio 2010) and FEEDBACKS (Prometeo – Generalitat Valenciana). EUPHORE instrumentation is partly funded by the Spanish Ministry of Science and Innovation, through INNPLANTA project: PCT-440000-2010-003. LV is supported by the Max Planck Graduate Center with the Johannes Gutenberg-Universität Mainz (MPGC).

Open Access Article. Published on 06 January 2015. Downloaded on 5/6/2026 12:57:53 PM.
This article is licensed under a Creative Commons Attribution 3.0 Unported Licence.

Notes and references

1 R. L. Mauldin III, T. Berndt, M. Sipilä, P. Paasonen, T. Petäjä, S. Kim, T. Kurtén, F. Stratmann, V.-M. Kerminen and M. Kulmala, *Nature*, 2012, **488**, 193.
2 G. Sarwar, K. Fahey, R. Kwok, R. C. Gilliam, S. J. Roselle, R. Mathur, J. Xue, J. Yu and W. P. L. Carter, *Atmos. Environ.*, 2013, **68**, 186.
3 P. Forster and V. Ramaswamy, *et al.*, *IPCC 4*, 2007, ch. 2, vol. 160.
4 R. A. Cox and S. A. Penkett, *Nature*, 1971, **230**, 321.
5 R. Criegee and G. Wenner, *Liebigs Ann. Chem.*, 1949, **564**, 9.
6 D. Johnson and G. Marston, *Chem. Soc. Rev.*, 2008, **37**, 699.
7 H. Niki, P. D. Maker, C. M. Savage, L. P. Breitenbach and M. D. Hurley, *J. Phys. Chem.*, 1987, **91**, 941.
8 R. I. Martinez and J. T. Herron, *J. Phys. Chem.*, 1987, **91**, 946.
9 G. T. Drozd, J. Kroll and N. M Donahue, *J. Phys. Chem. A*, 2011, **115**, 161.
10 G. T. Drozd and N. M Donahue, *J. Phys. Chem. A*, 2011, **115**, 4381.
11 M. S. Alam, A. R. Rickard, M. Camredon, K. P. Wyche, T. Carr, K. E. Hornsby, P. S. Monks and W. J. Bloss, *J. Phys. Chem. A*, 2013, **117**, 12468.
12 K. Izumi, M. Mizuochi, K. Murano and T. Fukuyama, *Atmos. Environ.*, 1987, **21**, 1541.
13 J. G. Calvert, R. Atkinson, J. A. Kerr, S. Madronich, G. K. Moortgat, T. J. Wallington and G. Yarwood, *The Mechanisms of Atmospheric Oxidation of the Alkenes*, Oxford University Press, New York, 2000.
14 C. A. Taatjes, G. Meloni, T. M. Selby, A. J. Trevitt, D. L. Osborn, C. J. Percival and D. E. Shallcross, *J. Am. Chem. Soc.*, 2008, **130**, 11883.
15 O. Welz, J. D. Savee, D. L. Osborn, S. S. Vasu, C. J. Percival, D. E. Shallcross and C. A. Taatjes, *Science*, 2012, **335**, 204.
16 C. A. Taatjes, O. Welz, A. J. Eskola, J. D. Savee, A. M. Scheer, D. E. Shallcross, B. Rotavera, E. P. F. Lee, J. M. Dyke, D. W. K. Mok, D. L. Osborn and C. J. Percival, *Science*, 2013, **340**, 177.
17 D. Stone, M. Blitz, L. Daubney, N. U. M. Howes and P. Seakins, *Phys. Chem. Chem. Phys.*, 2014, **16**, 1139.
18 B. Ouyang, M. W. McLeod, R. L. Jones and W. J. Bloss, *Phys. Chem. Chem. Phys.*, 2013, **15**, 17070.
19 T. Berndt, T. Jokinen, R. L. Mauldin III, T. Petaja, H. Herrmann, H. Junninen, P. Paasonen, D. R. Worsnop and M. Sipila, *J. Phys. Chem. Lett.*, 2012, **3**, 2892.
20 L. Vereecken, H. Harder and A. Novelli, *Phys. Chem. Chem. Phys.*, 2012, **14**, 14682.
21 J. R. Pierce, M. J. Evans, C. E. Scott, S. D. D'Andrea, D. K. Farmer, E. Swietlicki and D. V. Spracklen, *Atmos. Chem. Phys.*, 2013, **13**, 3163.
22 M. Olzmann, E. Kraka, D. Cremer, R. Gutbrod and S. Andersson, *J. Phys. Chem. A*, 1997, **101**, 9421.
23 A. Novelli, L. Vereecken, J. Lelieveld and H. Harder, *Phys. Chem. Chem. Phys.*, 2014, **16**, 19941.
24 K. T. Kuwata, M. R. Hermes, M. J. Carlson and C. K. Zogg, *J. Phys. Chem. A*, 2010, **114**, 9192.
25 J. T. Herron, R. I. Martinez and R. E. Huie, *Int. J. Chem. Kinet.*, 1982, **14**, 201.
26 J. D. Fenske, A. S. Hasson, A. W. Ho and S. E. Paulson, *J. Phys. Chem. A*, 2000, **104**, 9921.
27 J. H. Kroll, S. R. Sahay, J. G. Anderson, K. L. Demerjian and N. M. Donahue, *J. Phys. Chem. A*, 2001, **105**, 4446.
28 J. M. Beames, F. Liu, L. Lu and M. I. Lester, *J. Am. Chem. Soc.*, 2012, **134**, 19104.
29 J. M. Beames, F. Liu, L. Lu and M. I. Lester, *J. Chem. Phys.*, 2013, **138**, 244307.
30 K. H. Becker, *EUPHORE: Final Report to the European Commission, Contract EV5V-CT92-0059*, Bergische Universität, Wuppertal, Germany, 1996.
31 M. S. Alam, M. Camredon, A. R. Rickard, T. Carr, K. P. Wyche, K. E. Hornsby, P. S. Monks and W. J. Bloss, *Phys. Chem. Chem. Phys.*, 2011, **13**, 11002.
32 T. Berndt, T. Jokinen, M. Sipilä, R. L. Mauldin, H. Herrmann, F. Stratmann, H. Junninen and M. Kulmala, *Atoms. Environ.*, 2014, **89**, 603.
33 S. M. Saunders, M. E. Jenkin, R. G. Derwent and M. J. Pilling, *Atmos. Chem. Phys.*, 2003, **3**, 161.
34 H. Niki, P. D. Maker, C. M. Savage and L. P. Breitenbach, *J. Phys. Chem.*, 1981, **85**, 1024.
35 S. Hatakeyama, H. Kobayashi and H. Akimoto, *J. Phys. Chem.*, 1984, **88**, 4736.
36 O. Horie and G. K. Moortgat, *Atmos. Environ., Part A*, 1991, **24**, 1881.
37 P. Neeb, O. Horie and G. K. Moortgat, *Int. J. Chem. Kinet.*, 1996, **28**, 721.
38 A. S. Hasson, G. Orzechowska and S. E. Paulson, *J. Geophys. Res.*, 2001, **106**, 34131.
39 A. R. Rickard, D. Johnson, C. D. McGill and G. Marston, *J. Phys. Chem. A*, 1999, **103**, 7656.
40 H. Niki, P. D. Maker, C. M. Savage and L. P. Breitenbach, *Chem. Phys. Lett.*, 1977, **46**, 327.
41 R. A. Cox and S. A. Penkett, *J. Chem. Soc., Faraday. Trans.*, 1972, **68**, 1735.
42 H. G. Kjaergaard, T. Kurtén, L. B. Nielsen, S. Jørgensen and P. O. Wennberg, *J. Phys. Chem. Lett.*, 2013, **4**, 2525.
43 L. Vereecken, H. Harder and A. Novelli, *Phys. Chem. Chem. Phys.*, 2014, **16**, 4039.
44 C. A. Taatjes, O. Welz, A. J. Eskola, J. D. Savee, D. L. Osborn, E. P. F. Lee, J. M. Dyke, D. W. K. Mok, D. E. Shallcross and C. J. Percival, *Phys. Chem. Chem. Phys.*, 2012, **14**, 10391.
45 O. Welz, A. J. Eskola, L. Sheps, B. Rotavera, J. D. Savee, A. M. Scheer, D. L. Osborn, D. Lowe, A. Murray Booth,

Open Access Article. Published on 06 January 2015. Downloaded on 5/6/2026 12:57:53 PM.
This article is licensed under a Creative Commons Attribution 3.0 Unported Licence.

P. Xiao, M. Anwar H. Kahn, C. J. Percival, D. E. Shallcross and C. A. Taatjes, *Angew. Chem., Int. Ed.*, 2014, **18**, 4547.
46 T. Berndt, J. Voigtländer, F. Stratmann, H. Junninen, R. L. Mauldin III, M. Sipilä, M. Kulmala and H. Herrmann, *Phys. Chem. Chem. Phys.*, 2014, **16**, 19130.
47 A. B. Ryzhkov and P. A. Ariya, *Phys. Chem. Chem. Phys.*, 2004, **6**, 5042.
48 Y. Scribano, N. Goldman, R. J. Saykally and C. Leforestier, *J. Phys. Chem. A*, 2006, **110**, 5411.
49 L. Sheps, A. M. Scully and K. Au, *Phys. Chem. Chem. Phys.*, 2014, **16**, 26701.
50 J. M. Anglada, J. Gonzalez and M. Torrent-Sucarrat, *Phys. Chem. Chem. Phys.*, 2011, **13**, 13034.
51 W. Adam, R. Curci and J. O. Edwards, *Acc. Chem. Res.*, 1989, **22**, 205.
52 R. W. Murray, *Chem. Rev.*, 1989, **89**, 1187.
53 R. Curci, A. Dinoi and M. F. Rubino, *Pure Appl. Chem.*, 1995, **67**, 811.
54 D. Heard, *Nature*, 2012, **488**, 164.
55 J. Prousek, *Chem. Listy*, 2009, **103**, 271.
56 C. A. Taatjes, D. E. Shallcross and C. J. Percival, *Phys. Chem. Chem. Phys.*, 2013, **16**, 1704.